RSC Advances

PAPER

View Article Online
View Journal | View Issue

Cite this: *RSC Adv.*, 2023, **13**, 36168

Microbial corrosion behavior of pipeline steels in simulation environment of natural gas transportation pipeline†

Lixia Zhu,[ac] Yufei Tang,[*ab] Junyi Jiang,[a] Yuxuan Zhang,[a] Mingxiao Wu,[d] Chen Tang,[ab] Tao Wu[ab] and Kang Zhao[ab]

Bacteria are introduced into natural gas transmission pipelines through water-driven gas extraction, which can exacerbate the occurrence of pipeline corrosion. This study utilized a micro-reactor to design a simulated corrosion environment that mimics natural gas gathering and transportation pipelines. The objective was to investigate the corrosion behavior of X80 pipeline steel under the combined effects of CO_2, Cl-, sulfate reducing bacteria (SRB), and iron bacteria (IOB). Additionally, it aimed to elucidate the influence mechanisms of these two microorganisms on corrosion. Under a humid environment with a total pressure of 8.5 MPa and a partial pressure of CO_2 at 0.85 MPa, the corrosion rate of X80 pipeline steel was observed to follow the sequence: IOB > control (asepsis) > SRB + IOB > SRB. During the initial stages of corrosion, highly active IOB becomes the primary factor contributing to corrosion. As corrosion progresses, the concentration of dissolved oxygen in the SRB system gradually decreases while SRB activity intensifies, leading to the formation of FeS through the process of corrosion. The corrosion current density (i_{corr}) exhibited a significant decrease, thereby intensifying localized corrosion of the corrosion products beneath the film. This resulted in a maximum pitting depth of 113.5 μm. Research on the behavior of microbial-enhanced corrosion provides significant guidance in the development and implementation of protective coatings.

Received 12th October 2023
Accepted 5th December 2023

DOI: 10.1039/d3ra06940k

rsc.li/rsc-advances

1 Introduction

Given the uneven distribution of energy resources and unique geographical conditions, long-distance transportation of oil and gas is essential. Pipelines serve as crucial infrastructure for efficient gathering and transportation of these materials.[1,2] During the pipeline gathering process, natural gas commonly contains impurities including free water, H_2S, and CO_2, which can corrode the inner wall of the pipeline.[3–5] The occurrence of CO_2 corrosion on the inner surface of pipelines used for natural gas gathering and transportation is a prevalent form of acid corrosion.[6,7] Acid corrosion was first reported in a Texas well in 1940, and since then, it has remained a persistent issue in various oil fields worldwide.[8,9] In the oil and gas industry, over 950 000 wells are characterized as acidic, constituting approximately one-third of all wells.[10] Moreover, water drive is commonly employed in the development of gas fields to enhance their economic benefits.[11–13] Besides utilizing recycled industrial water, treated sewage is employed for reinjection into pipelines.[14] Despite the treatment of industrial circulating water and oilfield reinjection water, a small number of microorganisms still persist.[15,16] In favorable temperature conditions, these microorganisms (such as SRB (Sulfate Reducing Bacteria) and IOB (Iron-Oxidizing Bacteria)) continue to proliferate, leading to microbial corrosion and exacerbating pipeline deterioration. The occurrence of pipeline corrosion perforation leading to oil and gas leakage not only disrupts transportation but also results in environmental pollution, resulting in significant economic losses and environmental challenges.[17]

The process of microbial corrosion encompasses various disciplines such as materials science, chemistry, electrochemistry, microbiology, and others.[18,19] Microbial growth, reproduction, and decline directly and indirectly contribute to the perpetual instability of material surfaces, rendering microbial corrosion a highly intricate process.[20–22] Previous studies conducted in laboratory settings have examined the corrosion caused by various bacteria, such as SRB and IOB.[23,24] The insolubility of metallic materials necessitates that oxidation reactions, such as iron oxidation, take place extracellularly. Consequently, transportation of electrons from outside the cell to the cytoplasm becomes essential for a reduction reaction.[25]

[a]*Department of Materials Science and Engineering, Xi'an University of Technology, Xi'an 710048, PR China. E-mail: yftang@xaut.edu.cn*

[b]*Shaanxi Province Key Laboratory of Corrosion and Protection, Xi'an University of Technology, Xi'an 710048, PR China*

[c]*CNPC Tubular Goods Research Institute, Xi'an 710077, PR China*

[d]*State Grid Henan Electric Power Research Institute, Nanyang 450099, PR China*

† Electronic supplementary information (ESI) available. See DOI: https://doi.org/10.1039/d3ra06940k

For instance, sulfate-reducing bacteria utilize iron as an electron donor and sulfate as an electron acceptor in biofilm-associated sessile communities. This necessitates the transfer of electrons to accomplish the REDOX process.[26] Initially, electrons generated through extracellular metal oxidation are transferred from the metal surface to cytochrome on the cell wall. Subsequently, they enter the cell to engage in the intracellular respiration's electron transport chain.[27] Additionally, microbial corrosion can occur as a result of corrosive metabolites secreted by microorganisms. Acidophilic bacteria (APB), for instance, have the ability to generate organic acids that create an adequately acidic environment within their biofilm. Microorganisms, both aerobic and anaerobic, have the capability to generate sufficient amounts of organic acids, leading to microbiologically influenced corrosion. Despite the application of an organic protective coating[28] within the pipe, microorganisms can still target and degrade organic substances like plasticizers and polymers. Microorganisms produce enzymes that break down organic compounds like plasticizers and polymers, allowing them to acquire small organic molecules as a source of nutrients.[29]

Microbiologically influenced corrosion becomes more intricate when there are small concentrations of oxygen present, as oxygen typically serves as the final electron acceptor.[30] For example, Iron-Oxidizing Bacteria (IOB), which is a common type of metal-oxidizing bacteria, employ O_2 as an electron acceptor during respiration.[31] This metabolic pathway catalyzes the transformation of Fe^{2+} to Fe^{3+}, elevates the valence state of iron, and enables CO_2 fixation to acquire organic carbon. The presence of a significant concentration of Fe^{3+} ions at the interface of carbon steel leads to their precipitation as $Fe(OH)_3$, which subsequently forms a layer of corrosion products. The presence of a $Fe(OH)_3$ film layer creates an anode zone, leading to galvanic corrosion. Electrons are then directly transferred from FeO to oxygen in the cathode zone, resulting in the formation of OH^-. Ultimately, this process leads to the development of pitting pits on the surface of carbon steel. The uneven adhesion of microorganisms on the metal surface results in a biofilm that exhibits a patchy distribution on the metal surface during later stages.[32] Through respiration, aerobic bacteria release oxygen from the subbiofilm area, resulting in the formation of sites characterized by low oxygen concentrations.[33] Consequently, these regions transform into anode locations due to their relatively higher oxygen content compared to surrounding areas, resulting in localized oxygen corrosion. Conversely, the regions lacking sufficient biofilm coverage exhibit elevated levels of oxygen concentration and serve as cathode regions where electron consumption reduces the presence of oxygen.[34]

At present, anaerobic and aerobic bacteria may co-exist in complex natural gas working conditions and play a synergistic role in corrosion. How their activity changes and how it affects corrosion need to be further studied. Therefore, the effects of SRB and IOB alone and together on the microbial corrosion of X80 pipeline steel under high pressure CO_2 transport in the pipeline were studied. The corrosion behavior of X80 pipeline steel surface was studied by means of average corrosion rate, XRD, SEM, microbial activity and three-dimensional imaging, and the microbial corrosion kinetics was analyzed by electrochemical tests such as OCP, EIS and polarization curve. Furthermore, the microbial corrosion mechanism of X80 pipeline steel in different environments was elucidated. These findings hold significant implications for designing effective materials to protect against microbial corrosion in natural gas pipelines.

2 Experimental section

2.1 Materials

X80 pipeline steel (Dongguan Chengju Metal Material Co., LTD, Guangdong) was used as experimental material. The size of the X80 pipeline steel sample is 40 mm × 10 mm × 3 mm. To prepare the sample, it was first scrubbed with acetone to eliminate any surface oil. It was then cleaned using ethanol and purged with N_2 before being placed in a drying dish for future utilization. Sulfate-Reducing Bacteria (SRB) and Iron oxiding bacteria are both extracted from the soil of the oil and gas field in the southwest of China.[35] Sodium chloride (NaCl, analysis pure, Tianjin Damao Chemical Reagent Factory, Tianjin) and deionized water were used to prepare 3.5% NaCl solution as a corrosive medium.

2.2 Experimental procedure

To replicate the real operating conditions within a natural gas transmission pipeline, a micro-reactor (YZQR-500, Yanzheng Instrument (Shanghai) Co., Ltd) was utilized to create a high-pressure CO_2 quasi-static environment. The pre-treated pipeline steel sample was placed in the reactor, and the bacterial culture medium (containing 10^4 bacteria per mL, the bacteria were SRB and IOB) and 3.5% NaCl were added until the surface of the sample was not exceeded, and the joint action of CO_2, Cl^-, SRB and IOB in the corrosion process was studied. Sterile conditions served as the control group. Nitrogen gas (N_2) was introduced into the miniature reactor at a pressure of 3 MPa and held at that pressure for 3 minutes. This process was repeated three times to ensure complete removal of air from the miniature reactor. The mixture of CO_2 and O_2/N_2, with a partial pressure of 0.085 MPa, was sequentially introduced into the micro-reactor. This sequential introduction was done to maintain a CO_2/O_2 partial pressure ratio of 1 : 1. Subsequently, N_2 is introduced into the reactor until it reaches a pressure of 8.5 ± 0.1 MPa, while simultaneously adjusting the internal temperature of the reactor to 40 ± 1 °C. Corrosion samples of pipeline steel were collected at intervals of 1, 3, 6, 9, 12, and 15 days. All the aforementioned procedures are conducted within a sterile environment. Prior to usage, utensils utilized in microbial experiments, as well as X80 pipeline steel and NaCl solution, must undergo a 20 minutes disinfection process under a UV lamp to eradicate any potential presence of bacteria.

2.3 Characterization

The corrosion rate of the sample was determined using the weight loss method. A rust removal liquid for iron-based materials is formulated in accordance with the specifications

outlined in GB/T16545-2015. Prior to conducting the corrosion experiment, the sample was weighed and subsequently immersed in a rust removal solution. Following a predetermined corrosion time, it underwent ultrasonic treatment for 10 min. Next, the surface of the sample was washed with deionized water for 20 S and then dehydrated in anhydrous ethanol for 10 min. Following that, the samples were placed in a vacuum drying oven at 60 °C for 3 h and subsequently dried in a drying dish for 24 h before undergoing another weighing process. Average corrosion rate is calculated according to the formula in JB/T 7901-2001. The two mass differences are recorded as ΔM, and the average corrosion rate (Vc) is calculated by the following formula,

$$\mathrm{Vc} = \frac{87600 \times \Delta M}{\rho \times S \times T} \quad (1)$$

where ΔM represents the weight difference before and after corrosion (g), ρ denotes the sample density (g cm^{-3}), S indicates the surface area of the specimen (cm^2), and T represents the corrosion time (h).

The phase composition of the corrosion products in the sample was analyzed using an XRD-7000 X-ray diffractometer equipped with the following parameters: a Cu target, Kα radiation with a wavelength (λ) of 1.54059 Å, a tube voltage of 40 kV, a tube current of 40 mA, a scanning range from 10° to 80°, and a scanning rate of 8° min^{-1}. Following corrosion, the sample was immersed in a 2.5% glutaraldehyde solution ($C_5H_8O_2$, Tianjin Hengxing Chemical Reagent Factory) and then fixed at a temperature of 4 °C for a duration of 8 hours. Subsequently, the sample underwent a gradual dehydration process using anhydrous ethanol with concentrations of 50%, 70%, 80%, 90%, and finally, pure (100%) ethanol. Following the drying of the sample, a layer of gold was applied *via* spraying, and the resulting corrosion morphology was examined using a VEGA3 XMU scanning electron microscope. The AO/EB double staining reagent (Beijing Solaibao Technology Co., LTD) was utilized to stain the bacteria present on the sample's surface following bacterial corrosion. Subsequently, the sample was immersed in a sterile culture solution for 5 min, with this process being repeated three times prior to staining. The dyeing reagent consisted of AO : EB in a ratio of 1 : 1, and the duration of dyeing ranged from 3 to 5 min. The fluorescent inverted microscope (CKX53, Olympus Corporation) was employed to assess the viability of bacteria on the sample's surface. Dead bacteria were visualized in red, while live bacteria appeared green. DSX-500 (Olympus, Tokyo, Japan) automatic three-dimensional imaging microscope was used to observe the surface morphology of X80 pipeline steel after removing corrosion products, and 2D and 3D images were obtained in bright field (BF) mode.

The electrochemical test was conducted using the CS-310H electrochemical workstation. A 50 mL three-hole electrolytic cell was utilized for the experiment. The working electrode consisted of the corrosion sample under investigation, while a Pt electrode served as the auxiliary electrode. The reference electrode employed was a saturated AgCl electrode. The pipe steel samples were taken out of the micro-reactor after corrosion for 1 d, 3 d, 6 d, 9 d, 12 d, and 15 d respectively. Before the electrochemical test, the insulated copper wire was welded to the back of the X80 pipeline steel specimen, mounted with epoxy resin and the working surface (10 mm × 10 mm) was retained. The sample was placed in the test system for open circuit potential testing for 30 minutes until its open circuit potential became stable (Fig. S1†). For the Electrochemical Impedance Spectroscopy (EIS) test, a sinusoidal disturbance signal with an amplitude of 10 mV was applied and the frequency range of the test was 0.01 to 100 000 Hz. The test voltage range of the polarisation curve is −0.2 to 0.2 V, and the sampling rate is 0.5 mV s^{-1}.

3 Results and discussion

3.1 Microbial corrosion rate of X80 pipeline steel

The average corrosion rate of X80 pipeline steel after 1–15 days of exposure to different bacterial systems under a high-pressure CO_2 environment is illustrated in Fig. 1. The corrosion behavior of X80 pipeline steel is generally consistent across various bacterial systems. During the initial stage of corrosion, the highest corrosion rates were observed in the four bacterial systems: 0.586 mm a^{-1}, 0.5115 mm a^{-1}, 0.5812 mm a^{-1}, and 0.6382 mm a^{-1}, respectively. The maximum initial corrosion rate is attributed to the complete exposure of the X80 pipeline steel to the corrosive medium, without any coverage of corrosion products or biofilms on its surface. The average corrosion rate significantly decreases as the corrosion time prolongs. This phenomenon is attributed to the formation of corrosion products on the surface of the sample as well as the development of a biofilm, both contributing to a reduction in the dissolution rate of pipeline steel. During the middle and later stages of corrosion, the average corrosion rate of the samples in all four bacteria-containing systems exhibited an initial increase followed by stabilization. On the 15th day, the corrosion rates of X80 pipeline steel in the four bacterial systems were measured as follows: 0.3656 mm a^{-1} for IOB, 0.2657 mm a^{-1} for control, 0.4187 mm a^{-1} for SRB + IOB, and 0.3321 mm a^{-1} for SRB. In

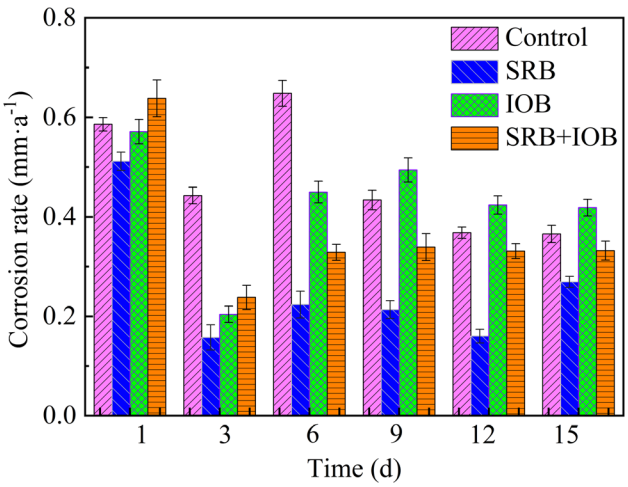

Fig. 1 Average corrosion rates of X80 pipeline steel in different microbial environments.

the IOB system, the corrosion of X80 pipeline steel is influenced not only by IOB but also by a synergistic effect between a N_2 + CO_2 + O_2 gas mixture at a total pressure of 8.5 MPa and Cl^-. This synergistic effect leads to the highest corrosion rate observed within the IOB system. The increase in dissolved oxygen content in a high-pressure NaCl solution intensifies the effect of O_2 corrosion within this system. Additionally, since IOB is an oxygen-loving bacterium, an elevated level of dissolved oxygen in the solution allows IOB to sustain high activity.[36] This, in turn, enhances bacterial adhesion onto the surface of X80 pipeline steel and facilitates biofilm formation. Among all corrosion cycles, the average corrosion rate of samples in the IOB containing system is the highest, and the average corrosion rate in the SRB system is lower than that in the other three systems. The average corrosion rate of samples in the SRB system is 0.2234 mm a^{-1} at day 6, which is about 49.7% of that in the SRB system. The average corrosion rate of samples in aseptic system was 1.38 times higher than that in SRB system. The average corrosion rate of SRB + IOB system was between IOB and SRB system, but lower than that of aseptic system, indicating that the synergistic action of the two microorganisms significantly inhibited the corrosion behavior of X80 pipeline steel under this working condition.

3.2 Effects of different bacteria bearing conditions on the composition and morphology of corrosion products

Fig. 2 illustrates the phase composition of corrosion products on X80 pipeline steel across various bacterial environments. The composition of corrosion products showed no significant variation across the four bacterial environments, with the predominant presence of FeO, Fe_2O_3, Fe_3O_4, $FeCO_3$, FeO(OH), and $Fe(OH)_3$. Notably, in the SRB system, the appearance of a diffraction peak corresponding to FeS on day 15 suggests a persistently low activity of sulfate-reducing bacteria. Furthermore, characteristic corrosion products only manifested during the later stages of corrosion. Upon completion of various corrosion periods, the naked eye observation reveals the presence of adhered corrosion products on the surface of X80 pipeline steel across different systems. Following 6 days of corrosion, the IOB group samples exhibited a substantial buildup of dark brown corrosion products on their surfaces. The resulting corrosion product layer resembled a protective "shell," suggesting the formation of a relatively intact biofilm by iron bacteria on the surface of X80 pipeline steel within the same timeframe. The corrosion products consist of intermediate compounds such as FeO, Fe_2O_3, and Fe_3O_4, which are formed through dehydration of FeOOH and $Fe(OH)_3$. Additionally, $FeCO_3$ is identified as a product of CO_2 corrosion. The extent of CO_2 corrosion in this operating condition is significantly influenced by the ambient temperature and partial pressure of CO_2, which are maintained at low levels. A lower ambient temperature results in a higher Ksp($FeCO_3$), leading to gradual dissolution of any $FeCO_3$ film that may be present. The influence of CO_2 partial pressure on corrosion is contingent upon its solubility in water. In natural gas pipelines, where wet gas or limited liquid is present, solubility is affected. A decrease in CO_2 partial pressure leads to reduced solubility and subsequently lowers the concentration of decomposed H^+ ions from H_2CO_3, weakening cathode depolarization. Consequently, under specific temperature and CO_2 partial pressure conditions within this environment, only a small quantity of $FeCO_3$ forms as part of the corrosion products.

The microscopic morphology of X80 pipeline steel after 7 days of corrosion in various bacterial environments under high CO_2 pressure was examined, and the findings are presented in Fig. 3. The inset in the upper right corner provides a magnified view. In the absence of bacteria, the surface corrosion product film on X80 pipeline steel comprises an outer rust layer and an inner rust layer. However, the thin outer rust layer does not provide complete coverage, resulting in tightly packed granular corrosion products forming a dense inner rust layer in areas where it is absent. In the presence of SRB (sulfate-reducing bacteria), numerous voids emerged within the corrosion products on the surface of the pipeline steel. Upon magnification, it was further evident that the corrosion layer exhibited a layered structure with porous regions. These pores have the potential to facilitate the penetration of corrosive Cl^- ions through the corrosion product layer, establishing contact with the underlying metal volume and promoting more severe pitting corrosion.[37] The influence of high pressure on IOB corrosion medium results in an increased concentration of dissolved oxygen, thereby enhancing the corrosive activity during the initial and middle stages. Additionally, due to the nodulation characteristic exhibited by IOB during the corrosion process, a substantial quantity of corrosion products can be generated (Fig. 3(c)). Consequently, a compact iron oxide film develops on the surface of X80 pipeline steel. Once this dense corrosion product film is established, unbound IOB present in the corrosive medium persistently adheres and actively contributes to corrosion, resulting in the formation of granular corrosion products. In environments where both SRB (Sulfate-Reducing Bacteria) and IOB (Iron-Oxidizing Bacteria) coexist, the primary corrosion products formed on sample surfaces consist mainly of an internal rust layer, resulting in a loosely porous structure. Upon magnification, it becomes evident that these corrosion products exhibit a morphology akin to that observed in IOB systems. This similarity indicates that IOB-induced corrosion predominates during the early and middle stages within this environment. However, due to SRB adhesion on metal matrix surfaces, numerous micropores are formed. Moreover, as these micropores become further covered by a corrosion product film, they create a relatively anaerobic microenvironment conducive to SRB activity enhancement.[38] Consequently, this leads to exacerbation of localized point corrosion.

3.3 Microbial corrosion mechanism with high pressure CO_2 transport

According to the average corrosion rate, the phase composition of corrosion products and the morphology of corrosion products, the corrosion mechanism of X80 pipeline steel under different bacteria containing conditions was analyzed, as shown in Fig. 4. During the initial corrosion stage of the control group

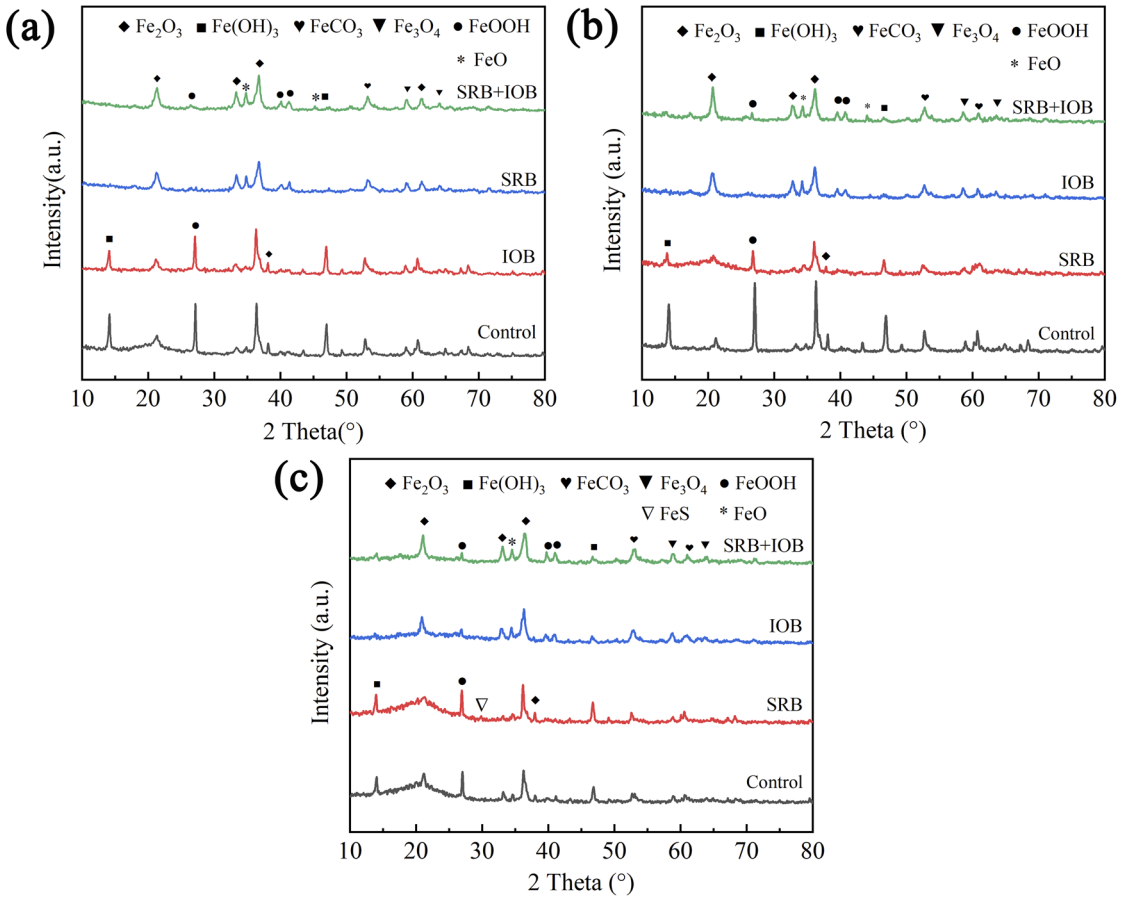

Fig. 2 Corrosion product compositions of X80 pipeline steel in microbial environments at different times: (a) 3 days, (b) 6 days, (c) 15 days.

(Fig. 4(a)), the combined influence of Cl^-, CO_2, and O_2 in the thin layer solution enhances the cathodic polarization process. Consequently, this impact affects the anodic reaction occurring on the surface of X80 pipeline steel, leading to an accelerated dissolution rate of Fe^{2+}. In this system, the cathodic process of corrosion is caused by the hydration of CO_2 and the reduction of O_2 in water. Due to high pressure, the concentrations of HCO_3^-, CO_3^{2-} and dissolved oxygen in the thin layer solution increase, and the cathodic reactions involved are as follows.

$$CO_2 + H_2O \rightarrow H_2CO_3 \quad (2)$$

$$2H_2CO_3 + 2e^- \rightarrow H_2 + 2HCO_3^- \quad (3)$$

$$2HCO_3^- + 2e^- \rightarrow H_2 + 2CO_3^{2-} \quad (4)$$

$$O_2 + 4e^- + 2H_2O \rightarrow 4OH^- \quad (5)$$

The anode reaction in the system is:

$$Fe \rightarrow Fe^{2+} + 2e^- \quad (6)$$

The total chemical reaction is:

$$CO_2 + 1/2O_2 + 2H_2O + 2Fe \rightarrow FeCO_3 + Fe(OH)_2 + H_2 \quad (7)$$

This acceleration of the anodic dissolution process results in continuous generation of Fe^{2+}, which reacts with OH^- and CO_3^{2-} to form $Fe(OH)_2$ and $FeCO_3$. With the continuous formation of $Fe(OH)_2$, $FeCO_3$ and other products, the solubility of these products in the corrosion system is limited, resulting in the deposition of corrosion products on the pipeline steel surface. Among them, the corrosion product is $Fe(OH)_2$, which is then oxidized to the unstable $Fe(OH)_3$. Subsequently, $Fe(OH)_3$ is transformed into FeOOH, and finally FeOOH is dehydrated to form the final corrosion product Fe_2O_3.

$$Fe(OH)_3 \rightarrow FeOOH + H_2O \quad (8)$$

$$2FeOOH \rightarrow Fe_2O_3 + H_2O \quad (9)$$

At the initial stage of corrosion, the surface of X80 pipeline steel is completely exposed in the corrosion system, and the interaction process of ion interface is accelerated during the corrosion period, and the corrosion product film is formed rapidly. However, in the middle stage of corrosion, the passivation film is destroyed, leading to continuous submembrane corrosion, which is the reason why the corrosion product film consists of an outer rust layer and an inner rust layer. At the later stage of corrosion, with the intensive accumulation of granular Fe_2O_3, $FeCO_3$ and other products, a complete

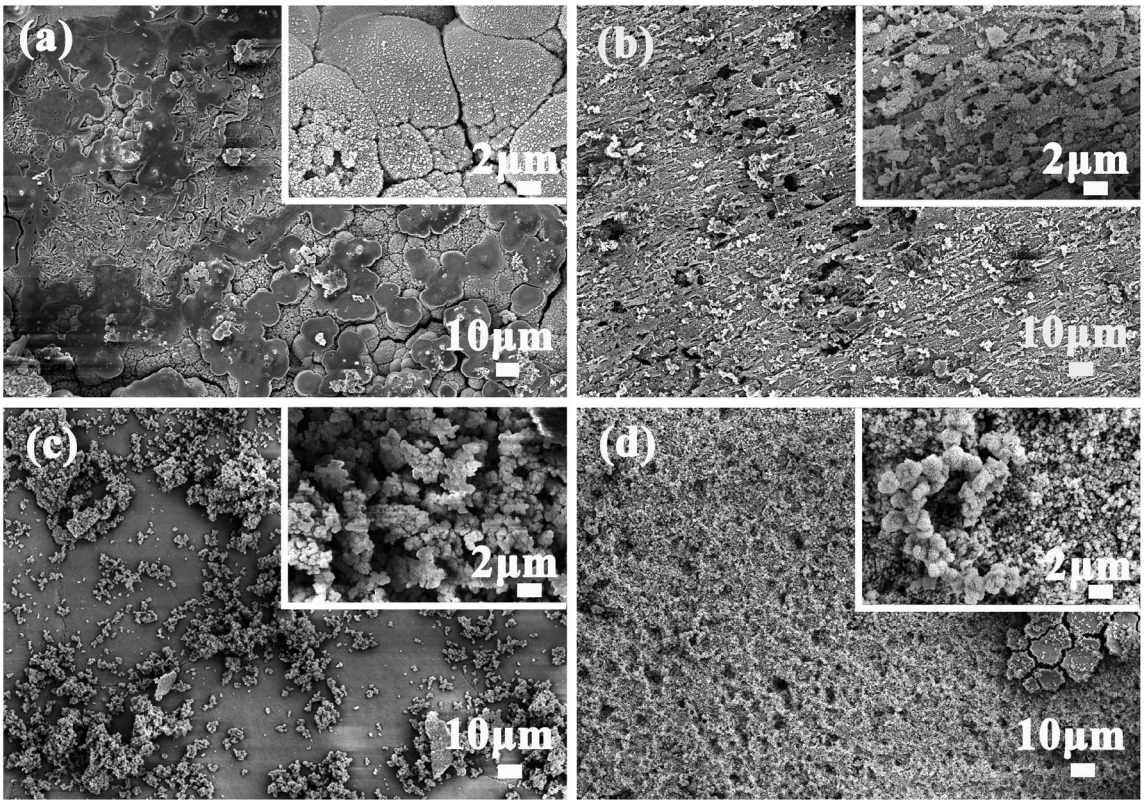

Fig. 3 Morphologies of surface corrosion products of X80 pipeline steel in different microbial environments: (a) control, (b) SRB, (c) IOB, (d) SRB + IOB. Insert images show magnifications.

passivation film is formed, and it is more difficult for Cl^- to penetrate the corrosion products. Finally, there is no deep pitting pit on the surface of X80 pipeline steel, and its corrosion type is dominated by uniform corrosion.

Fig. 4(b) shows the corrosion mechanism of X80 pipeline steel induced by SRB in CO_2 high-pressure environment. At the initial stage of corrosion, dissolved oxygen in thin layer solution became the preferred oxidizer for corrosion of X80 pipeline steel in corrosion system. The presence of O_2 reduces both the number and activity of free SRB. Consequently, this mechanism results in a lower corrosion rate for X80 pipeline steel compared to other bacterial systems. In the middle stage of corrosion, the SRB biofilm is covered with a large number of corrosion products produced by CO_2/O_2, which creates a relatively anaerobic environment for the SRB fixed on the surface of X80 pipeline steel and promotes the fixed SRB activity. Due to the small radius of Cl^- and strong penetration ability, the passivation film is easy to penetrate and break, and then form a large cathode (passivation film) and a small anode (metal matrix), resulting in pitting. With the catalytic effect of extracellular polymer (EPS) produced through Cl^- and SRB metabolism, the anode metal undergoes continuous dissolution, resulting in the progressive expansion and deepening of pitting corrosion.

The anodic reaction still involves the oxidation process of Fe. In the later stages of corrosion, the dissolved oxygen in the thin layer solution is significantly depleted, leading to further enhancement of SRB activity. Additionally, SRB utilizes Fe as an electron donor and SO_4^{2-} as an electron acceptor, reducing SO_4^{2-} to S^{2-}. The main mechanism of SRB action involves the formation of H_2S and precipitation of FeS. This leads to the formation of iron sulphide (Fe_xS_y) under the corrosion product film, which acts as an electrochemical coupling between the cathode and the exposed steel substrate (anode), exacerbating the corrosion of the steel. Thus, the accumulation of metabolized sulphides further accelerates the corrosion process of X80 pipeline steel in SRB systems. This is also considered to be the main factor contributing to the maximum depth of pitting observed in X80 pipeline steel.

The corrosion mechanism of X80 pipeline steel in IOB environments is illustrated in Fig. 4(c). Upon attachment to the metal surface, IOB rapidly generates a significant amount of Fe_2O_3 deposits. Therefore, during the initial stages of corrosion, the influence of IOB leads to the rapid formation of a Fe_2O_3 product film on the surface of X80 pipeline steel. As corrosion progresses, IOB maintains high activity and facilitates the anodic dissolution of the pipeline steel surface. The dissolved Fe^{2+} diffuses into the thin layer solution and undergoes further oxidation to Fe^{3+}. The Fe^{3+} generated from IOB oxidation may react with Cl^- to form highly corrosive ferric chloride solution, which can concentrate beneath rust nodules (corrosion product clusters). In the thin layer solution, hydrolysis of $FeCl_3$ occurs, resulting in the formation of $Fe(OH)_3$ and H^+, leading to an

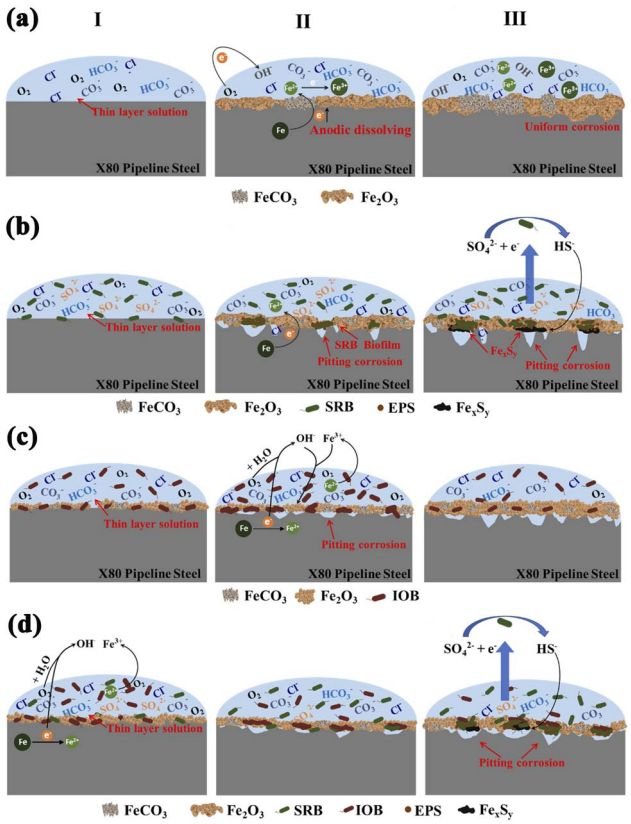

Fig. 4 Corrosion mechanisms of X80 pipeline steel in different microbial environments: (a) control, (b) SRB, (c) IOB, (d) SRB + IOB. I, II and III represent the early, middle and late stages of corrosion respectively.

acidic corrosive solution. This is also a primary reason for the highest corrosion rate observed in X80 pipeline steel within IOB systems. The formation of a thicker corrosion product film on the surface of X80 pipeline steel and a decrease in the oxygen concentration required for IOB metabolism in the thin layer solution contribute to reduced IOB activity during later stages of corrosion. At this stage, the corrosion product film acts as a protective barrier for X80 pipeline steel, slowing down ion exchange processes at the corrosion interface.

Fig. 4(d) presents a schematic diagram illustrating the corrosion mechanism of X80 pipeline steel under the influence of a mixed culture of SRB and IOB in a high-pressure CO_2 environment. During the initial stages of corrosion, the high dissolved oxygen concentration in the thin layer solution and the elevated activity of IOB play significant roles. Therefore, during this stage, IOB dominates the corrosion process of X80 pipeline steel. Phase analysis also confirms that the corrosion products mainly consist of Fe_2O_3 and FeOOH. As IOB grows and metabolizes, aerobic IOB respiration consumes O_2, providing better growth conditions for anaerobic SRB. SRBs attach to the metal substrate by penetrating through gaps in the corrosion products, forming a composite biofilm. Within this biofilm, SRBs generate sufficient corrosive H_2S, which lowers the local pH and leads to severe localized corrosion.

3.4 Bacterial activity on X80 pipeline steel surface with different corrosion time

Fluorescence microscopy is a tool that utilizes fluorescent dyes to stain intracellular substances, enabling cells to exhibit coloration under specific light, thus facilitating qualitative or semi-quantitative studies on cellular substance transport and distribution. X80 pipeline steel samples were subjected to staining of adhered bacteria on the surface after being placed in four corrosion systems: control, SRB, IOB, and SRB + IOB, for different durations. The results of bacterial activity are shown in Fig. 5, where green represents live bacteria and red represents dead bacteria. In the SRB system, during the early and middle stages of corrosion (1 day, 3 days, 6 days), there were relatively few viable SRBs on the surface of X80 pipeline steel. However, at 12 days, a large number of green dots appeared, indicating an increase in SRB activity during the later stage of corrosion when the microenvironment within the corrosion system changed favorably for their survival. In the IOB system, the variation pattern of bacterial quantity on the surface of X80 pipeline steel exhibited an initial growth followed by a decline trend, with the highest number of green dots observed at 6 days. In the subsequent corrosion cycles, the dissolved oxygen content in this corrosion system gradually decreased, resulting in the inhibition of IOB metabolic activity. The number of red dots on the sample surface gradually increased, and at 15 days, a large number of dead bacteria adhered to the surface. In the SRB + IOB system, the bacterial activity on the surface of X80 pipeline steel exhibited higher levels during both the early and later

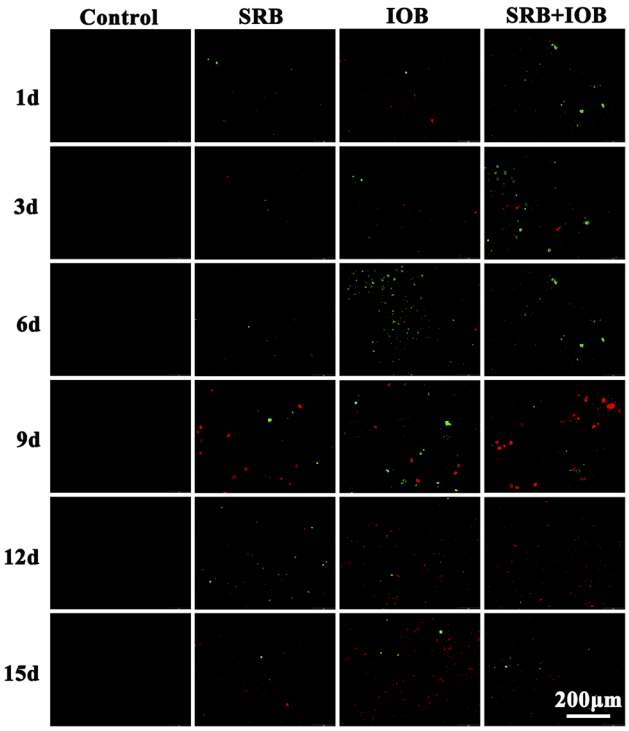

Fig. 5 Bacterial activities on the surface of X80 pipeline steel after corrosion for 1, 3, 6, 9, 12 and 15 days in different microbial environments. Red indicates dead bacteria, green indicates live bacteria.

stages of corrosion, with only a few green dots observed at 9 and 12 days. This may be attributed to initially high IOB activity. As corrosion time prolonged, the remaining viable IOBs on the sample surface decreased gradually, accompanied by a reduction in dissolved oxygen content within the microenvironment, thereby providing favorable anaerobic conditions for SRB growth. It can be inferred that post-corrosion exhibited high bacterial activity predominantly by sulfate-reducing bacteria. Due to the high-pressure and low-liquid environment inside natural gas pipelines, it is not conducive for microbial adhesion and subsequent growth metabolism to form biofilms. Therefore, from the figure, significant areas of biofilm have not been observed yet.

3.5 Pitting morphology and depth of X80 pipeline steel with different bacteria conditions

X80 pipeline steel corrodes in different bacterial systems, and bacteria will adhere to the surface of the sample, and the contact between the sample and bacteria causes changes in the microenvironment on the surface of the sample (such as pH, dissolved oxygen, and HCO_3^- plasma concentration), and the irregular adhesion of bacteria causes corrosion pits on the surface of X80 pipeline steel. Fig. 6 shows the pitting morphology of X80 pipeline steel after removal of surface corrosion products and biofilm after corrosion in control, SRB, IOB, and SRB + IOB systems for 15 days. In the control group, there are very few pitting pits on the surface of the sample, which is due to the high pressure effect that increases the HCO_3^- concentration in the corrosion system. The surface of X80 pipeline steel presented dense pitting pits under the other three bacteria containing systems, among which the number of pitting pits on the surface of samples under the IOB system was the largest, followed by the SRB + IOB system, and the number of pitting pits in the SRB system was the least. This is also positively correlated with the bacterial proliferation and metabolic activities on the surface of X80 pipeline steel. IOB maintains a high bacterial activity during the entire corrosion cycle, while SRB produces fewer pitting pits because oxygen content in the microenvironment inhibits its metabolic proliferation.

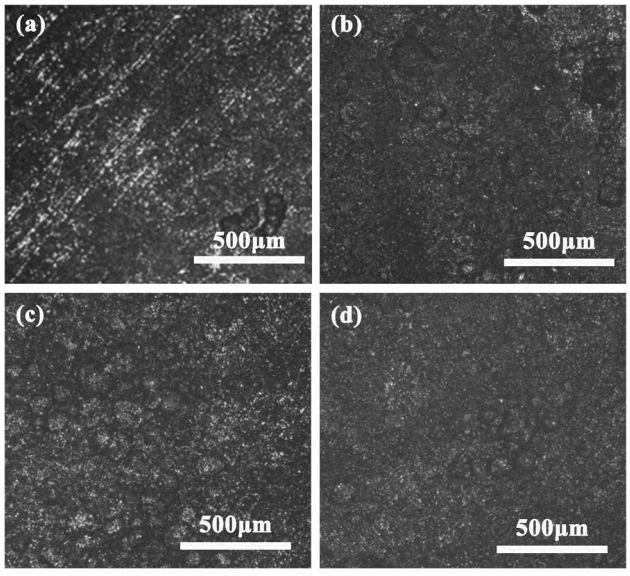

Fig. 6 Surface pitting morphologies of X80 pipeline steel after corrosion for 15 days in different microbial environments: (a) control, (b) SRB, (c) IOB, (d) SRB + IOB.

Fig. 7 shows the three-dimensional image of X80 pipeline steel corroded under four systems for 15 days after removing surface corrosion products and biofilm, which further characterized the pitting depth and the number of pitting pits on the sample surface. In the control group, X80 pipeline steel is mainly uniform corrosion, and the maximum corrosion depth is 38.8 μm, which is mainly caused by CO_2, Cl^- and a small amount of dissolved oxygen in the corrosion system. However, the surface corrosion depth of samples in the three bacteria-containing systems was much greater than that in the control group, among which the maximum corrosion depth of samples in the IOB system was 79.1 μm, and that in the SRB + IOB system was 76.4 μm. The maximum corrosion depth of SRB system was 113.5 μm, which was higher than that of the other two bacterial systems and 2.9 times that of the control group. The joint action of SRB and Cl^- in corrosive medium can greatly increase the pitting tendency of X80 pipeline steel surface. With the extension of corrosion time, the SRB adhesion on the surface of X80 pipeline steel gradually increased. The reduction of SRB accelerates the cathode reaction rate in the microzone, and finally accelerates local corrosion, resulting in pitting pits.

3.6 Electrochemical analysis

With the prolongation of corrosion time, the adhesion of corrosion products and biofilm will affect the surface properties of X80 pipeline steel, and then affect the electrochemical behavior of the sample. OCP is a non-destructive electrochemical test method that reflects the change of electrode surface potential, and can be used for preliminary qualitative analysis of microbial corrosion to a certain extent. Generally, the increase of OCP indicates that the anode reaction is inhibited or the cathode reaction is promoted. In contrast, the decrease of OCP value indicates that the anode reaction is promoted or the cathode reaction is inhibited. Fig. 8 shows the transformation curve of open potential (OCP) of X80 pipeline steel with corrosion time in control, SRB, IOB, SRB + IOB systems. The open circuit potential of samples in control, SRB, IOB and SRB + IOB systems showed a positive trend, but there were differences in potential changes. At 1 day, the open circuit potential of control, SRB and IOB systems remained around −0.582 V, and the OCP of the IOB system increased significantly to 0.019 V and tended to be stable at 3 days, and increased to 0.203 V at 15 days. The OCP of the SRB system remained at a low potential level in the first 6 days, and increased to −0.001 V at the 9th day. In the later stage of corrosion, the OCP continued to increase and finally reached 0.209 V. The OCP value of the SRB + IOB system changed slightly and increased slowly over time, from the initial −0.072 V to 0.179 V. OCP values increased in all systems, indicating that the cathodic reaction during corrosion was promoted.

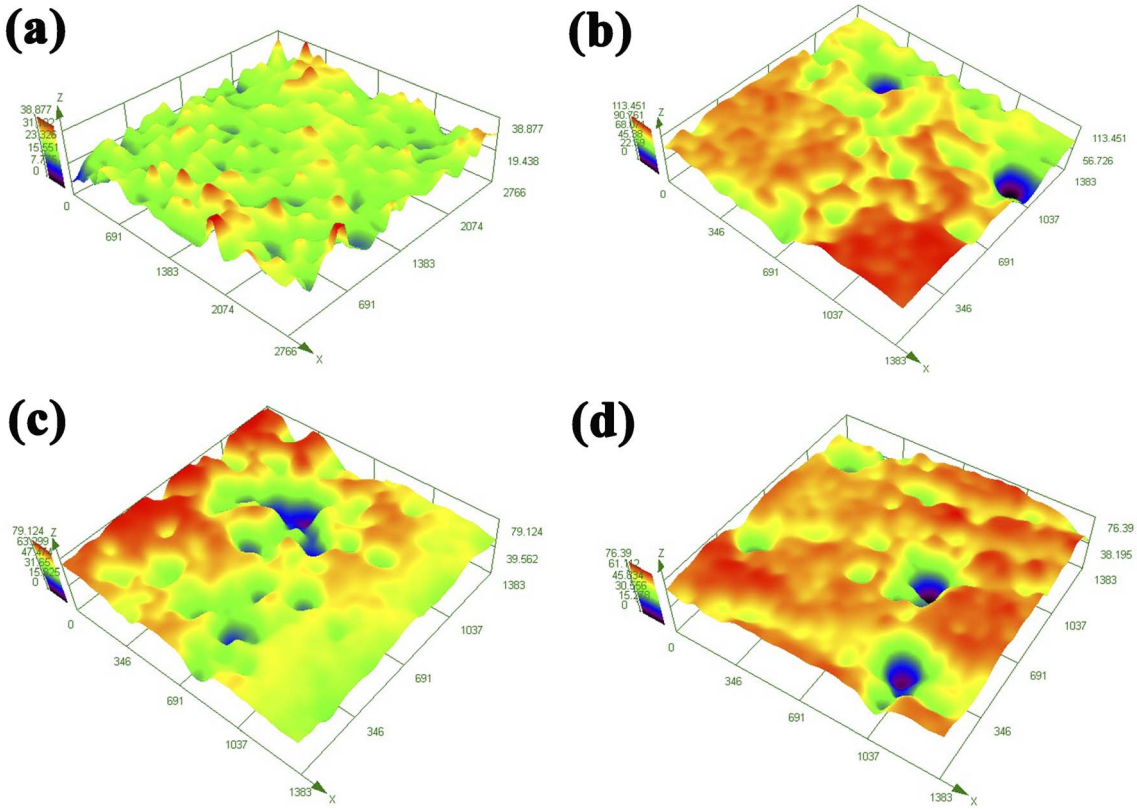

Fig. 7 Surface 3D image of X80 pipeline steel after corrosion for 15 days in different microbial environments: (a) control, (b) SRB, (c) IOB, (d) SRB + IOB.

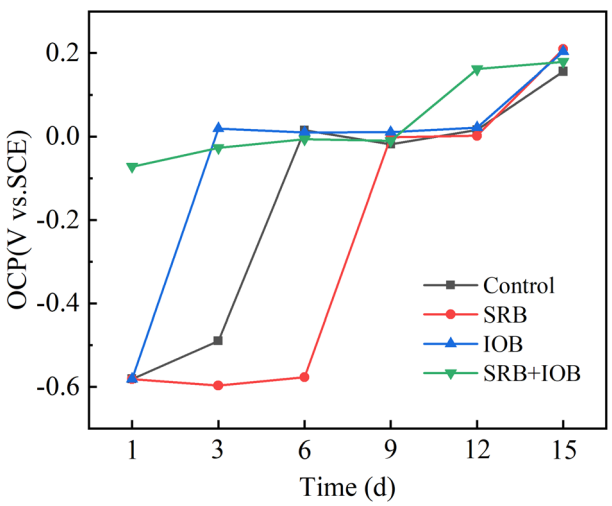

Fig. 8 Open circuit potentials of X80 pipeline steel after corrosion for 1, 3, 6, 9, 12 and 15 days in different microbial environments.

Fig. 9(a)–(d) show Nyquist plots of electrochemical impedance spectra of X80 pipeline steel in four corrosion systems. The Nyquist curve is "arc-shaped", showing that the impedance arc is caused by the formation of corrosion products on the sample surface. The radius of Nyquist arc is usually used to evaluate the interface charge transfer resistance between the corroded medium and the sample. The change of the radius of the impedance arc indicates the increase or decrease of the surface impedance value of the corroded sample. When the radius of the impedance arc increases, the charge transfer resistance increases and the corrosion rate decreases. This phenomenon reflects the change of the state of the corrosion product film on the surface of the sample, and then affects the mass transfer rate of the corrosive substance to the metal matrix. The impedance changes of different bacterial systems were significantly different. In the control group, the impedance arc radius continues to increase from 1 to 6 days, and fluctuates within 6 to 15 days, first decreasing, then increasing and then decreasing. In this system, the average corrosion rate decreases first, then increases, and finally becomes stable, which is negatively correlated with the impedance arc change law. This is due to the deposition of corrosion products and defects on the surface of the sample. In the SRB system, the impedance arc radius continued to decrease from 1 to 6 days, increased from 6 to 12 days, and significantly decreased at 15 days. This was due to the increase of anaerobic bacteria activity at the later stage of corrosion, and the anaerobic biofilm on the surface of the sample increased the corrosion sensitivity of X80 pipeline steel, resulting in a significant decrease in the impedance arc. In the IOB system, the impedance arc radius of X80 pipeline steel increases with the increase of time, and the impedance reaches the maximum at 15 days. In this system, the impedance radius

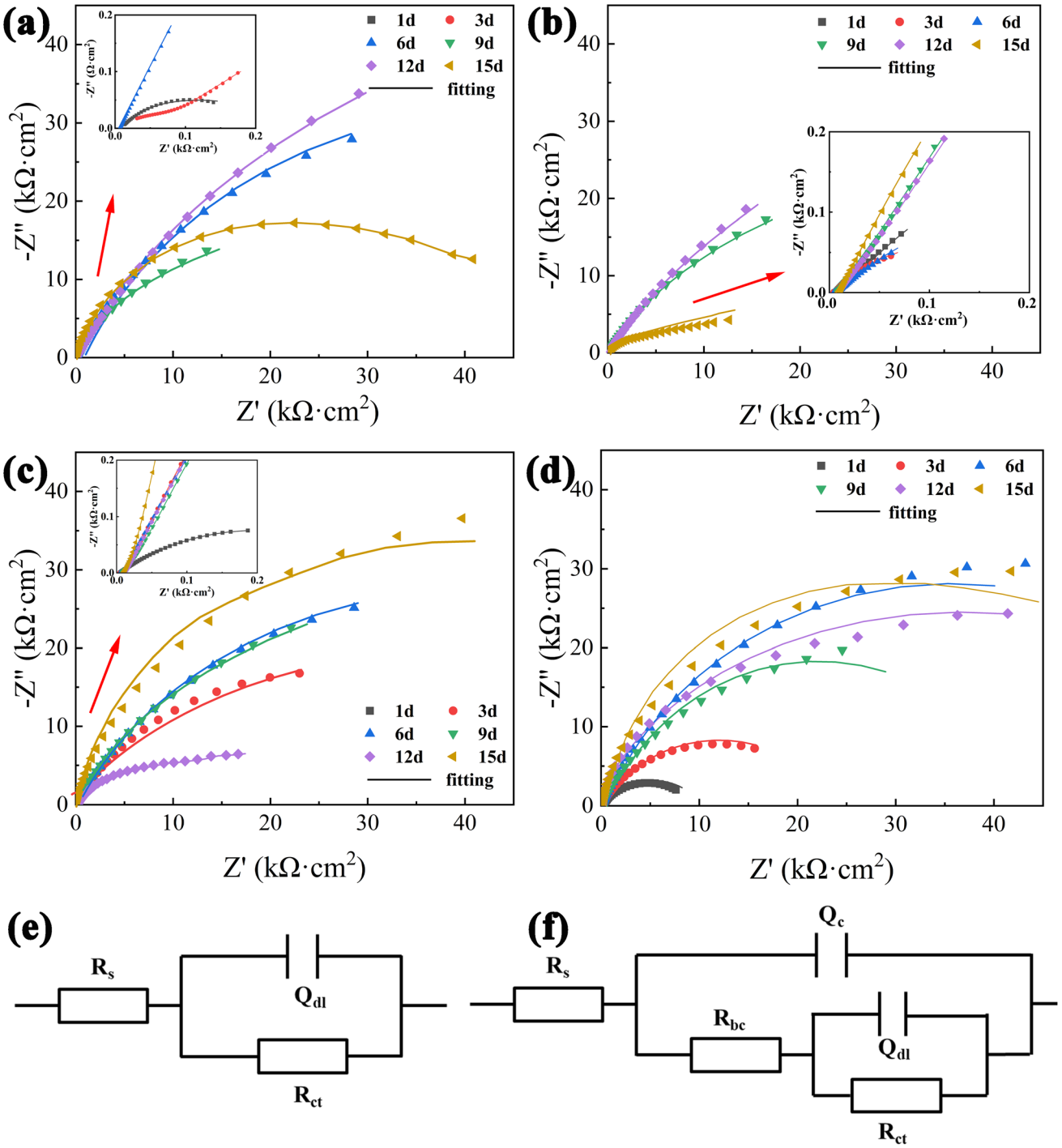

Fig. 9 Nyquist plots of X80 pipeline steel after corrosion for 1, 3, 6, 9, 12 and 15 days in different microbial environments: (a) control, (b) SRB, (c) IOB, (d) SRB + IOB, (e) equivalent circuit in control, (f) equivalent circuit in microbial environments.

of the corrosion product film and the biofilm are densely interlaced, and the impedance radius continues to increase. In the SRB + IOB system, the impedance arc radius increases from 1 to 6 days, decreases from 6 to 9 days, and continues to increase from 9 to 15 days. According to the change law of the impedance arc, the corrosion behavior in the system is mainly dominated by IOB. Although the impedance arc fluctuates during the corrosion stage, it generally shows an increasing trend.

In order to further analyze the electrochemical impedance spectroscopy data, CS Studio 6.5 software was used for circuit fitting, and the equivalent circuit models in Fig. 9(e) and (f) were selected. Among them, R_s represents solution resistance, R_{bc} represents corrosion product/biofilm resistance, R_{ct} represents

charge transfer resistance, Q_{bc} and Q_{dl} represent corrosion product/biofilm capacitance and double layer capacitance respectively. Fig. 9(e) applies to the early stage of the control group, and Fig. 9(f) applies to SRB, IOB, SRB + IOB systems and the middle and late stage of the control group. In the SRB system, the R_{ct} level remained low because there were fewer corrosion products in the early stage and no film was formed, but the results of bacterial activity showed that the SRB activity was low in the early stage, so the corrosion rate was slow. The SRB adsorption and the formation of corrosion product film lead to the increase of R_{ct} value with the extension of time. In the IOB system, the R_{ct} value firstly increased and then decreased with the prolongation of corrosion time, reached the maximum value at day 6 (R_{ct} = 91000 Ω cm^2), and gradually decreased at day 6–15, which was also consistent with the results of bacterial fluorescence activity.

Fig. 10 shows the polarization curves of X80 pipeline steel in control, SRB, IOB and SRB + IOB systems at the initial and later stages of corrosion. The corrosion potential E_{corr} and corrosion current density i_{corr} at different corrosion periods were calculated by Tafel curve extrapolation method. The variation of E_{corr} of corrosion potential can reflect the corrosion tendency. When the E_{corr} moves forward, it indicates that corrosion is more difficult to occur and has a certain corrosion resistance, and *vice versa*. However, the corrosion current density i_{corr} is positively correlated with the corrosion rate. Generally, the higher the corrosion current density, the faster the corrosion rate. At day 1, the corrosion potential of X80 pipeline steel in control, SRB and IOB systems remained at a low level, and the self-corrosion potential of the two single bacterial systems was lower than that of the sterile system, indicating that the samples in the single bacterial system were in the active state of metal ion dissolution and had a tendency to corrosion. However, since there was no interaction between the microbial adsorption and the sample surface at the initial stage, and the sample surface in the aseptic system was in direct contact with Cl^- in the system, the corrosion current density in the system was slightly higher than that in the single strain system at day 1, which was also consistent with the average corrosion rate. At day 15, the corrosion potential E_{corr} of the four bacteria containing system

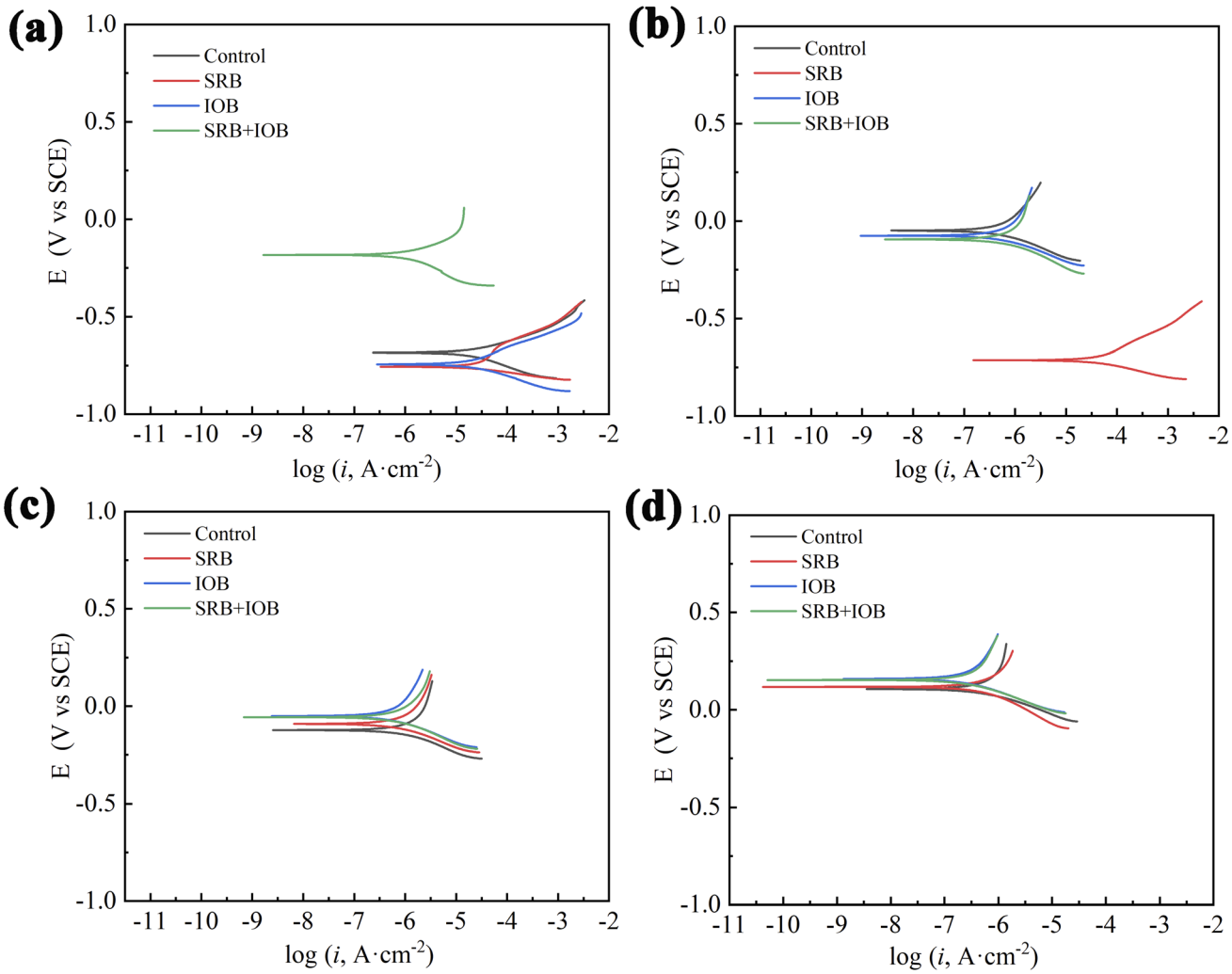

Fig. 10 Potentiodynamic polarization curves of X80 pipeline steel after corrosion for different time: (a) 1 day, (b) 6 days, (c) 9 days, (d) 15 days.

species X80 pipeline steel was positive, and the E_{corr} of IOB system was the largest, which was 0.15938 V, indicating that the corrosion product film completely covered the sample surface at day 15, preventing the further corrosion of Cl^- and HCO_3^- in the corrosion system on the sample. At this time, the minimum corrosion current density of X80 pipeline steel in the SRB system is 1.1128×10^{-7} A cm^{-2}, which indicates that the SRB activity increases in the later stage of corrosion, and the corrosion damage is further aggravated.

4 Conclusions

The microbial corrosion of X80 pipeline steel during high-pressure CO_2 transport was studied. The microbial corrosion rate of X80 pipeline steel in CO_2 high-pressure environment was found as follow: IOB > control > SRB + IOB > SRB. The high pressure forces the dissolved oxygen content to increase and the corrosion caused by IOB becomes severe in the early to middle period, resulting in a corrosion rate of 0.4187 mm a^{-1}. With the continuous consumption of dissolved oxygen in the later stage of corrosion, the corrosion of SRB was intensified, and the deepest pitting depth was 113.5 μm, which was 2.9 times that of the control group (the aseptic system). The predominant corrosion products on the surface of X80 pipeline steel in various systems are primarily Fe_2O_3 and $FeCO_3$, while the SRB system exhibits a minor presence of FeS as a corrosion product. During the later stage of corrosion, there was an increase in SRB activity, resulting in a minimum corrosion current density (i_{corr}) of 1.1128×10^{-7} A cm^{-2}, which subsequently exacerbated the corrosion process.

Conflicts of interest

There are no conflicts to declare.

Acknowledgements

This work was supported by National Natural Science Foundation of China (grant number 52172073) and Key Research and Development Program of Shaanxi (grant number 2020GY-264).

References

1 S. Conley, G. Franco, I. Faloona, D. R. Blake, J. Peischl and T. B. Ryerson, *Science*, 2016, **351**, 1317–1320.
2 Z. Liu, W. Tian, B. Liu and Z. Cui, *Eng. Appl. Artif. Intell.*, 2023, **121**, 106010.
3 M. G. Chesnokova, V. V. Shalaj, Y. A. Kraus, N. V. Cherkashina and A. Y. Mironov, *Procedia Eng.*, 2016, **152**, 247–250.
4 P. Guraieb and Q. Wang, Trends in Oil and Gas Corrosion Research and Technologies, in *Corrosion and scale at high pressure high temperature*, ed. A. M. El-Sherik, Elsevier Ltd, 2017, pp. 431–451.
5 S. Nešić, *Corros. sci.*, 2007, **49**, 4308–4338.
6 S. K. Kairy, S. Zhou, A. Turnbull and G. Hinds, *Corros. Sci.*, 2023, **214**, 110986.
7 X. Huang, L. Zhou, Y. Li, Z. Du, Q. Zhu and Z. Han, *Eng. Fail. Anal.*, 2023, **146**, 107079.
8 T. A. Jack and J. Szpunar, *Corros. Sci.*, 2023, **218**, 111196.
9 B. Wei, Q. Qin, Y. Bai, C. Yu, J. Xu, C. Sun and W. Ke, *Eng. Fail. Anal.*, 2019, **105**, 156–175.
10 Y. T. Al-Janabi and H. A. Al-Ajwad, *Corrosion*, NACE International, 2015.
11 E. Entezari, J. L. G. Velázquez, M. A. Mohtadi-Bonab, D. R. López, M. A. B. Zúñiga, R. K. Z. Davani and J. Szpunar, *Eng. Fail. Anal.*, 2023, **154**, 107650.
12 L. Xu, G. Qiao, X. Gong, Y. Gu, K. Xu and F. Xiao, *J. Mater. Res. Technol.*, 2023, **25**, 4216–4230.
13 H. Liang, R. F. Schaller and E. Asselin, *J. Pipeline Sci. Eng.*, 2021, **1**, 137–147.
14 I. A. Avelino-Jiménez, L. Hernández-Maya, V. Larios-Serrato, L. Quej-Ake, H. Castelán-Sánchez, J. Herrera-Díaz, V. Garibay-Febles, J. N. Rivera-Olvera, G. Zavala-Olivares and I. Zapata-Peñasco, *J. Environ. Chem. Eng.*, 2023, **11**, 109413.
15 T. Gu, *J. Microb. Biochem. Technol.*, 2014, **6**, 68–74.
16 J. F. D. Stott, *Corros. Sci.*, 1993, **35**, 667–673.
17 X. Li, Q. Chen, C. Li, X. Zhang, G. Tong, P. Cui, L. Lu, Q. Ma, J. Yuan, A. Fu, C. Yin and Y. Feng, *Eng. Failure Anal.*, 2022, **140**, 106566.
18 R. Jia, D. Yang, D. Xu and T. Gu, *Front. Microbiol.*, 2017, **8**, 2335.
19 L. Fan, Y. Sun, D. Wang, Y. Zhang, M. Zhang, E. Zhou, D. Xu and F. Wang, *Corros. Sci.*, 2023, **223**, 111421.
20 M. Yazdi, F. Khan, R. Abbassi, N. Quddus and H. Castaneda-Lopez, *Reliab. Eng. Syst. Safe.*, 2022, **223**, 108474.
21 J. Tang, R. Guo, X. Zhang and X. Zhao, *Heliyon*, 2022, **8**, e12588.
22 U. Eduok, E. Ohaeri and J. Szpunar, *Mater. Sci. Eng. C.*, 2019, **105**, 110095.
23 C. Chandrasatheesh, J. Jayapriya, R. P. George and U. Kamachi Mudali, *Eng. Fail. Anal.*, 2014, **42**, 133–142.
24 T. Wu, M. Yan, L. Yu, H. Zhao, C. Sun, F. Yin and W. Ke, *Corros. Sci.*, 2019, **157**, 518–530.
25 Q. Zhang, J. Li, J. Liu, C. Yin, Y. Qi and J. Zhou, *Electroanal. Chem.*, 2023, **945**, 117680.
26 F. Guan, Z. Liu, X. Dong, X. Zhai, B. Zhang, J. Duan, N. Wang, Y. Gao, L. Yang and B. Hou, *Sci. Total Environ.*, 2021, **788**, 147573.
27 U. Schröder, *Phys. Chem. Chem. Phys.*, 2007, **9**, 2619–2629.
28 N. Yoshimoto, I. Wahyudhin Fathona and A. Yabuki, *Colloids Surf., A*, 2023, **662**, 130970.
29 J.-D. Gu, *Int. Biodeterior. Biodegrad.*, 2003, **52**, 69–91.
30 P. Zhang, D. Xu, Y. Li, K. Yang and T. Gu, *Bioelectrochemistry*, 2015, **101**, 14–21.
31 W. Liao, J. Yuan, X. Wang, P. Dai, W. Feng, Q. Zhang, A. Fu and X. Li, *Int. J. Electrochem. Sci.*, 2023, **18**, 100069.
32 M. Qin, K. Liao, Y. Mou, X. Hao, S. Zhang, M. Wang and Y. Huang, *Process Saf. Environ. Prot.*, 2023, **179**, 329–347.
33 L. El-Bassi, I. Ziadi, S. Belgacem, L. Bousselmi and H. Akrout, *Int. Biodeterior. Biodegrad.*, 2020, **150**, 104960.
34 T. J. Tidwell, R. D. Paula, M. Y. Smadi and V. V. Keasler, *Int. Biodeterior. Biodegrad.*, 2015, **98**, 26–34.

35 L. Zhu, Y. Tang, S. Cao, J. Jiang, C. Wu and K. Zhao, *Ceram. Int.*, 2023, **49**, 5543–5549.
36 Y. Yue, M. Lv and M. Du, *Mater. Corros.*, 2019, **70**, 1852–1861.
37 W. Zhou, W. Lan, X. Cao, H. Deng, Y. Yan and X. Hou, *Int. J. Electrochem. Sci.*, 2018, **13**, 1283–1292.
38 Y. Shu, M. Yan, Y. Wei, F. Liu, E.-H. Han and W. Ke, *Acta Metall. Sin.*, 2018, **54**, 1408–1416.